Supporting Information

Coil-Globule Transition of a Water-Soluble Polymer

*Jianyu Liu[1], Huazhang Guo[2], Qingjie Gao[1], Hongbin Li[3], Zesheng An[1], and Wenke Zhang[1]**

AUTHOR ADDRESS:

[1]State Key Laboratory of Supramolecular Structure and Materials, College of Chemistry, Jilin University, Changchun 130012, China.

[2]Institute of Nanochemistry and Nanobiology, Shanghai University, Shanghai 200444, China.

[3]Department of Chemistry, University of British Columbia, Vancouver V6T 1Z4, Canada.

KEYWORDS:

Coil-Globule Transition, Water-Soluble Polymer, Poly(*N*-isopropylacrylamide), Magnetic Tweezers.

Table of Contents

1. Materials and Methods

1.1 Chemicals

1-(3-(Dimethylamino)propyl)-3-ethylcarbodiimide hydrochloride (EDC-HCl), *N*-hydroxy-succinimide (NHS), (3-aminopropyl)-dimethoxy-methylsilane (APDMMS), Tween-20, glutaraldehyde, isopropyl acrylamide (NIPAM), and 4,4'-azobis(4-cyanovaleric acid) (ACVA) were purchased from Sigma-Aldrich. All aqueous solutions were prepared with high-purity deionized water. Amino-modified magnetic particles (Thermo Fisher Scientific, Inc.), Reference particles (Polysciences, Inc.), 4-Cyano-4-(ethylthiocarbonothioylthio) pentanoic acid chain transfer agent (CTA) was synthesized according to a previously reported procedure.[1] PNIPAM was synthesized using RAFT polymerization, and the synthetic scheme is shown in Figure S13. ^{1}H NMR spectra are shown in Figure S14. The molecular weight of the synthesized PNIPAM was determined by GPC, as shown in Figure S15. As shown in Figure S16, there was a strong absorption peak of trithiocarbonate at 308 nm, as indicated by the black line,[2] whereas no peak at 308 nm was observed in the red line. Therefore, we confirmed that trithiocarbonate was completely removed from PNIPAM-SH.

Magnetic particles were purchased from Thermo Fisher Scientific. Dynabeads® M-270 Amine are uniform, superparamagnetic beads (2.8 µm in diameter) were coated with a hydrophilic layer of glycidyl ether, the surface is activated with primary amine functionality with a short hydrophilic linker.

1.2 Synthesis and characterization of PNIPAM.

In a typical reaction, NIPAM (1.4994 g, 0.0133 mol), CTA (0.58 mg, 0.0022 mmol) and ACVA (3.08 mg, 0.011 mmol) were dissolved in 1.5 mL DMF. Then the solution was degassed for 15 min and the reaction was placed in oil bath at 70 °C for 30 h. The monomer conversion was determined by ^{1}H NMR in $CDCl_3$ (conv [NIPAM] = 97%), and the solution was dialyzed in acetone with a dialysis membrane (MWCO 8000 g/mol). The solvent (acetone) was then removed by rotary evaporation, and the product (P1) was dried under vacuum overnight (1.2 g).

To obtain the mercaptan-containing PNIPAM (P2), PNIPAM (0.03 g, 0.046 µmol of trithiocarbonate moieties) was dissolved in DMF (2 mL). Deoxygenated ethanolamine (0.03 mg, 0.46 µmol, 10 folds with respect to the trithiocarbonate moieties) was injected into this solution after degassing for 20 min. The reaction mixture was stirred for 2 h at room temperature under nitrogen atmosphere. Finally, the solution was precipitated in diethyl ether and dried under vacuum overnight (PNIPAM-SH, 0.022 g). 9.0 mg purified PNIPAM-SH was dissolved in 3 mL DMF. Then the solution was characterized by UV-vis spectroscopy.

The molecular weight of PNIPAM was determined using GPC-MALLS system: This GPC system comprised an Agilent 1260 Infinity II with a Shodex guard column (P8514-KD000DMF), two Shodex separation columns KD-803 (8 mm × 300 mm) and KD-805 (8 mm × 300 mm). Detection was made with a Wyatt DAWN8 laser light scattering detector (Wyatt Technology Corporation) and an Optilab refractive index detector (Wyatt Technology Corporation). DMF (HPLC grade, containing 0.1 M LiBr) was used as the eluent at a flow rate of 0.75 mL/min. Three independent measurements were performed on the PNIPAM sample. The average molecular weight and the cumulative weight fraction-molar mass are shown in Figure S15. The GPC results show the average molecular weight of 87 kg/mol (Mw/Mn 1.639), 83 kg/mol (Mw/Mn 1.708), and 90 kg/mol (Mw/Mn 1.619), respectively. The proportion of molecular weight above 200 kg/mol is 22.82%; 22.73%; 22.98. In other words, there is nearly 23% chance to stretch the chain beyond 446 nm (200000/113*0.252) in SMFS.

1.3 Preparation of the flow chamber for Magnetic tweezers.

The flow chamber was assembled using a protocol similar to that described in a previous study.[3] The amino-substrate was activated for 30 min using 5% glutaraldehyde in a 10 mM PBS (pH 7.4) solution. Then, 200 uL reference particles (50 times dilution) and the very low concentrations of HS-PNIPAM-COOH solution (< 10^{-15} g/ml) were added successively to the chamber and incubated for 30 min to covalently attach them to the substrate via aldimine condensation and a thioacetal reaction. The amino-modified magnetic particles (100 times dilution) were covalently tethered to the carboxyl end of PNIPAM in the presence of NHS and EDC. PBS buffer was used to remove unconnected material from the previous steps by rinsing. The chamber and particles were then blocked with blocking buffer (1% Tween-20, 10 mM PBS, pH 7.4) for 12 h to prevent polymer-particle and polymer-surface interfacial interactions. Blocking can effectively inhibit interfacial interactions, and an appropriate nonionic blocking solution does not affect the coil-globule conformation transition of the PNIPAM chain (Figs. S1 and S17).[4] Finally, the block buffer was changed to experimental buffer for single-molecule stretching experiments. The chemical procedures to bind the chain to the substrate and to the magnetic particle for MT experiments are shown in scheme S1.

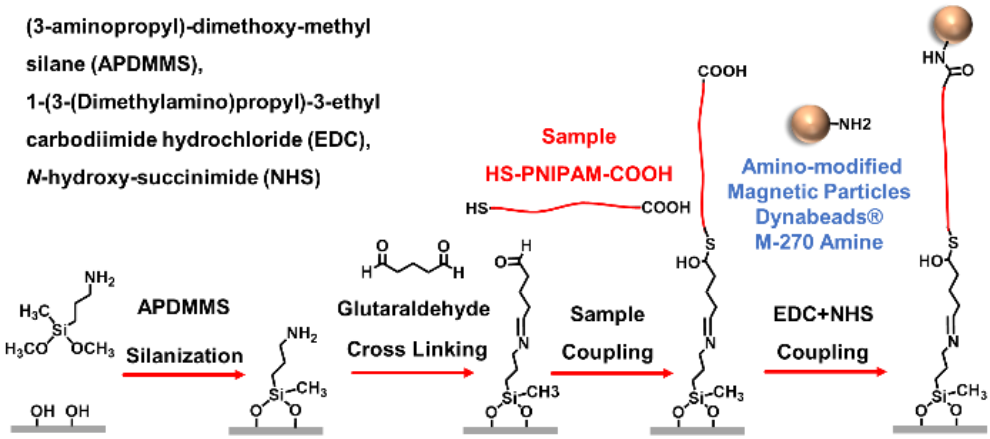

Scheme S1. The chemical procedures for immobilizing PNIPAM chain in between the magnetic particle and the glass substrate for MT experiments.

1.4 Magnetic tweezers experiments.

Magnetic tweezers (Biophysical Scientific Instrument Inc., Singapore) was used for single PNIPAM manipulation using a homemade sample-heating stage for temperature control (Figure S18). The temperature fluctuation range was within 0.5℃ (Figure S19). An SMFS experiment involving temperature-driven collapse (T) was performed at 42.5 ± 0.5℃ in 10 mM PBS, and that involving salt-driven collapse (S) was performed in a 0.3 M Na_2SO_4 solution at room temperature. The manipulation of PNIPAM was initiated after a stabilization time of at least 20 min. A scheme of MT setup is shown in Figure 1A. Using superparamagnetic particles, the pulling force was applied to the tethered PNIPAM chain. To improve the force accuracy, the force value of each manipulated molecule was further calibrated by the magnetic field function.[5] The force calibration had a relative error of <10%.[6] The loading rate was controlled by changing the height of the magnets according to previously published procedures. [3, 7] A constant-force experiments under two conditions (T, S) were carried out at a low force for 120 s to relax the polymer chains and at a high force for 600 s to unfold the collapsed chain, and the procedure was repeated. We also perform the same experiment with different chains. And these two cases have no detectable effect on our results. The three-dimensional coordinates (dx, dy, extension) of the magnetic particles with a polymer tether were recorded at a frequency of 200 Hz. The spatial resolution was ~2 nm by introducing the reference particles.[6] The change in 3D coordinates can reflect the attachment state and behavior of the polymer. Before the stretching experiment, the magnetic particle was rotated to determine the number of molecules attached between the magnetic particle and substrate. For the single-molecule tethered magnetic particles, the trajectory of the beads exhibited characteristic free rotation of a regular circle because of its uniform force in the x-y plane (Figure 1A, inset), whereas multiple-tethered particles show irregular movements (Figure S20).[8] When the polymer was occasionally adsorbed/detached to/from the surface, the 3D coordinates (dx, dy, extension) changed simultaneously (Figure S21). In contrast, when the structures of the polymer changed (coil-globule transition, Figure 1B), the center coordinates changed in only the z direction (Figure 1C and Figure S22). All polymers with interfacial interactions were excluded. For PNIPAM, the repeat unit number was calculated with respect to the backbone using a C-C bond length of 0.154 nm and a bond angle of 109.5° with a calculated repeat unit length of approximately 0.252 nm.[9] For data evaluation, OriginPro software (OriginLab Corporation, Northampton, Massachusetts, USA.) was used.

1.5 Magnetic tweezers instrument.

Magnetic tweezers instrument was purchased from Biophysical Scientific Instrument Inc., Singapore (Figure S18A). Magnetic setup was built based on Olympus IX73 inverted microscope.
Magnification of microscope: 100X, Olympus IX73 inverted microscope.
Thorlabs Collimated LED Light Sources for Olympus BX and IX Microscopes MCWHL5-C1.
Spatial resolution: 2 nm, PI PIFOC piezo nanofocusing Z drive.
Sampling rate: ≥200 frame per second, AVT Pike F-032B camera. Fast firewire camera for IX73 microscope with C-mount. Resolution: 640X480 pixels.

1.6 Temperature-controller of Magnetic tweezers.

Single molecule magnetic tweezers control the magnetic particle by a magnetic field, so it is necessary to avoid the interference of the heating coil electromagnetic field. Therefore, the heating coil is designed with symmetrical distribution to ensure that the magnetic fields were counteract each other. The heating coil (Figure S18C) is attached to the back of the microscope stage and heated from the bottom up.

1.7 Magnetic force calibration and error estimation.

1.7.1 Calculation of the force in the magnetic tweezers.

In magnetic tweezers experiments, one end of the tether is fixed to a surface, and the other end is attached to a paramagnetic bead. Force is generated by an external magnetic field toward its gradient. With enough number of data points collected (default number is 20000), the average and standard deviation of x, y, and z are calculated. The force is also calculated from the fluctuation along y direction and the extension (diameter of the paramagnetic bead is 2.8 um).

1.7.2 Force calibration.

To improve the force accuracy, the force value of each manipulated molecule was further calibrated by the magnetic field function.[5] The force calibration had a relative error of <10%.[6]

$$F=C*[\alpha_1*\exp(-d/\gamma_1) + \alpha_2*\exp(-d/\gamma_2)]$$

$$\alpha_1 = 1;\ \alpha_2 = 0.59755;\ \gamma_1 = 0.36477;\ \gamma_2 = 0.92278;$$

The d is the distance between the magnet and substrate and can be recorded by the instrument. The C is a heterogeneity parameter determined by the commercial magnetic particle.[5]

1.8 3D center position tracking with nanometer precision.

1.8.1 Magnetic bead fluctuation in x-y plane.

The y-position of the magnetic bead has a stable average value if the magnets are well aligned. On the other hand, x-location of the magnetic bead will jump when magnets move vertically along the force direction (Figure S1, S5, and S9). This is due to the rotation of magnetic beads when magnetic field and force change (Figure S10). In the x-z plane, the orientation of magnetic bead is determined by the torque balance of orientation-dependent magnetization of magnetic bead and the torque applied by the tension of the tether. The upward force is the magnetic force applied to the paramagnetic bead, while the downward force is the force applied by the tether which balances the magnetic force. The attaching point of the tether to the magnetic bead is often not at the right bottom of the magnetic bead, resulting in a non-zero torque. This torque tends to rotate the magnetic bead, but such rotation is restricted because the magnetic bead has a preferred orientation to align itself along the magnetic field. Magnetic field and magnetization of magnetic bead contributes another toque. The balance of the torques determines the final orientation of the magnetic bead.[5]

1.8.2 Determination of single- and multiple-molecule tethering

To visualize the stretching response of a single collapsed PNIPAM chain in real time, we monitor the 3D position of the magnetic particle attached to the end of a collapsed PNIPAM chain. The z value reflects the extension of the molecule along force direction, while x and y values reflect the transverse fluctuation of the magnetic bead. For the single-molecule tethered magnetic particles, the trajectory of the magnetic beads exhibited characteristic free rotation of a regular circle because of its uniform force in the x-y plane (Figure 1A, inset), whereas multiple-chain tethered particles show irregular movements (Figure S20).

1.8.3 Identification of interfacial desorption/adsorption during magnetic tweezers experiments.

After the single-molecule tethering is verified by trajectory of magnetic particles rotation, the source of the sudden extension jump is judged by the 3D coordinates of the molecular chain end. Because of the property of the magnetic field, the superparamagnetic particle is not subjected to magnetic force in the y-axis direction, the magnetic particles follow inverted pendulum motion in the y-axis direction and shows the y-axis center invariant feature (Figure 1C, Figure S1 and S21). When

an adsorbed polymer chain is detached from the substrate by the external force, the 3D coordinates (dx, dy, extension) change simultaneously due to movement characteristics (Figure S21). Because magnetic tweezers have high spatial accuracy (~2 nm), the desorption of a polymer chain from surface can be identified and excluded from the data analysis. For example, when adsorbed polymer chains dissociated toward the positive direction of the x-y axis (Figure S21A and S21B), the dx and dy suddenly increased. And when polymer chains dissociated toward the negative direction of the x-axis and the positive direction of the y-axis (Figure S21C and S21D), the dx suddenly decreased and dy suddenly increased.

1.9 Monitoring the coil-globule collapsing transition process of PNIPAM chain.

To observe the coil-globule transition in 0.3 M Na_2SO_4, the individual PNIPAM chain was unraveled at 6 pN external force then the external force was switched to 2 pN and kept at this value for around 2 minutes to allow the collapsing before the switch of the external force to 6 pN again. When the transition happened while the length of the polymer chain will get apparently shortened (Figure S9A). In addition, during the coil-globule transition, the collapsed curves of PNIPAM shows descending-and-wait steps as shown in yellow and green box (Figure S9B and S9C).

1.10 Unfolding of PNIPAM globule at a lower external force of 3 pN (R0-T3).

The manipulation procedure was the same as that unfolding at 6 pN (R0-T6) except decreasing unfolding force to 3 pN (R0-T3) at 42.5℃. The jump length j, waiting time τ, and slope s has not fundamentally changed in temperature-driven collapsed experiments. The jump length of primary nucleus is 8.0 ± 1.1 nm which is equivalent to 32 ± 4 repeat units. The lengths of bigger collapsed structures are still multiple of that of the nucleus (Supplementary Table 1). The collapsed method of PNIPAM did not change and still follow nucleation and adjacent mergence process under different unfolding force. The prior waiting time τ is the duration of a globule and reflects the globule's kinetic stability; it follows a multiexponential distribution, with at least two exponents, suggesting that either the kinetics of globule unfolding involves a multiple rate-limiting step. The average waiting time is ~ 8.4 s, corresponding to an ~0.12 s^{-1} unfolding rate, which is slightly lower than that measured at 6 pN unfolding force. This is expected because globule unfolding should be faster under higher pulling force. The expansive slope s still exhibits exponential distribution. **(**Figure S2 and S3).

1.11 Measurement parameters in magnetic tweezers

To extract the 3 parameters, jump length j, wait time τ and slope s for each wait-and-jump event in the extension-vs-time trajectories, we did the following:
(1) Smooth the original trajectory (gray) of a tethered magnetic bead using a percentile filter (Figure 1), which helps to reduce signal noise.
(2) Manually pick the start and end points of every possible jump using the smoothed trajectory (black). The identification of the jumps also gives the central position of magnetic beads and waiting time.
(3) Fit each waiting time period of the smoothed trajectory using a linear function, which intersects with the straight line of the jump (Figure 1 red). The slope of the linear fit of the waiting period is s.
(4) j, τ and t are defined in Figure 1, based on the trajectory after linear fitting (red line in Figure 1). j in nm (extension) is further converted to the number of repeat units.
(5) Only those jumps with a length larger than the two-time of z noise level (~4 nm) in the trajectory will be analyzed.

1.12 Calculation of end-to-end distance of PNIPAM.

The end-to-end distance in poor solvent is much smaller than the theoretical end-to-end distance. For example, for the nucleus, the theoretical end-to-end distance H = $\sqrt{nl^2}$ = $\sqrt{31 * 0.252^2}$ = 1.40 nm. The end-to-end distance in poor solvent is much smaller than the theoretical end-to-end distance H~1.40 nm, so the jump length was looked on as the actual size of the collapsed structure. When the number of merged nucleus reaches 8, the theoretical end-to-end distance H = $\sqrt{nl^2}$ = $\sqrt{248 * 0.252^2}$ = 3.97 nm, it is negligible relative to 64.7 nm.

1.13 Calculation on the number of repeat units within the jump length.

For PNIPAM, the number of repeat units was calculated with respect to the backbone using a C-C bond length of 0.154 nm and a bond angle of 109.5°with a calculated repeat unit length of around 0.252 nm.[9] The number of repeat units n = the jump length j / 0.252.

1.14 Calculation of the collapse rate (V).

As the magnet distance changes, first of all, the torque direction of the magnetic particle changes in x-z plane, and then the magnetic force applied to the magnetic particle changes. Therefore, for the accurate calculation of extension in the force change process, the height (extension) change caused by the torque change of the magnetic particles need to be deduced from the initial extension change. Therefore, we tethered the magnetic particles to the substrate through a very short chain (The elastic behavior of this short chain is negligible), and then scanned the height variation of torsion from 0 to 50 pN and established height correction curves of the magnetic particles' torsion (Figure S10). The measurement of extension variation (ΔExt) is 32.705 nm from 2 pN to 6 pN in the Figure S10B.

Subsequently, we counted 68 collapsed evets to calculate collapse rates. We take the data in Figure S9 as an example to illustrate the calculation process. For the first ramp as shown in Figure S9B, the collapse rate V_1 = (the extension variation +(ΔExt) / the waiting time = (-118.891+32.705) / 0.035 = -2462.46 nm/s. And for other ramp in Figure S9B, the collapse rate V_2 = the extension variation / the waiting time = -99.416 / 0.09 = -1104.62 nm/s; And for other ramp in Figure S9C, the collapse rate $V_{3\text{-}1}$ = -42.23 / 1.142 = -36.98 nm/s; $V_{3\text{-}2}$ = -11.205 / 0.24 = -46.69 nm/s; $V_{3\text{-}3}$ = -20.388 / 0.376 = -54.22 nm/s.

1.15 Sample preparations for AFM imaging.

1.15.1 Preparation of amino-modified substrate.

The silicon wafers (20 × 20 mm) were immersed in chloroform and anhydrous ethanol, sonicated for 10 min, rinsed with water, and dried with N_2. The silicon wafers were then treated with freshly prepared piranha solution (H_2SO_4 (98%)/H_2O_2 (30%) 7:3 v/v) for 10 min. After ultrasonic cleaning in water, the silicon wafers were washed with deionized water and dried in an oven at 115°C for 1 h. Subsequently, the silicon wafers were put into a desiccator filled with (3-aminopropyl)dimethylethoxysilane (APDMES, Fluorochem, U.K.) vapor for 30 min at 25°C. The silanized silicon wafers were washed three times with absolute methanol and activated in an oven at 115°C for 10 min.[3] AFM imaging shows there is no detectable aggregation on the amino-silanized substrates (Figure S11).

1.15.2 Immobilization and AFM imaging of PNIPAM molecules.

The amino-silanized substrate was activated for 30 min using 5% glutaraldehyde in 10 mM PBS (pH 7.4) solution. The activated substrate was rinsed by water. Then HS-PNIPAM-COOH (P2) solution (10^{-8} g/mL) were added successively to the chamber and incubated for 30 min to covalently attach them to the substrate via aldimine condensation and thioacetal reaction at room temperature. And then water is used to remove unconnected material from the previous step by through rinsing. It should be emphasized that water is a good solvent for PNIPAM at 25℃, and the low concentration (<10^{-8} g/mL) of PNIPAM exist in an isolated single-molecule state at 25℃. As described in the literature, the higher capability of a flexible polymer to spread produces an extremely flat profile as shown in the Figure S12D_1-D_5.[10] The individual polymers are indistinguishable from the substrate due to a height that is comparable to the substrate roughness and the finite dimensions of the tip.[10] Occasionally, a couple of collapsed single-chains due to dehydration can be detected. The collapsed beads appear around the center coiled chain, apparently without aggregation as shown in the Figure S12D_6.

2. Supplementary Figures

Section 2.1 Data collection and analysis for single molecule force spectroscopy

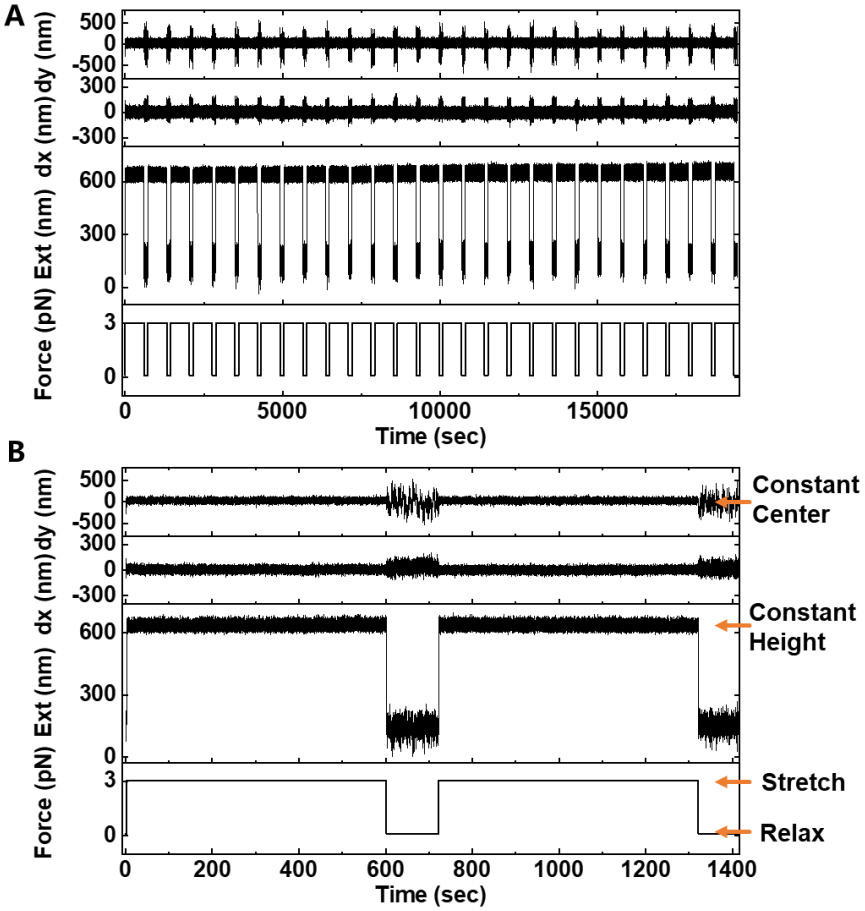

Figure S1. The 3D trajectory of PNIPAM chain under constant pulling force at room temperature (below LCST) in 10 mM PBS. (**A**) Typical traces obtained during multiple cycle of force jumping. (**B**) The enlarged view of the first two force jumping. The height of PNIPAM extension trace keeps constant at room temperature. Before temperature and salt driven transition, the constant force experiment of PNIPAM was performed at room temperature. The extension of PNIPAM does not exhibit sudden jump during stretching (3 pN), and the height of the extension remained the same (the center position at 634.6 nm) for 27 cycles under 3 pN force (Figure S1A). This is consistent with the expectation that PNIPAM chains does not collapse at room temperature. This also indicates that the sudden jump of the extension under the temperature and salt-driven collapsed condition results from the unfolding of collapsed structures. And the center positions of dy remain unchanged. The magnetic particles can be seen as inverted pendulum in the magnetic. Under small pulling force, the amplitude of inverted pendulum motion is high in the y-axis direction. On the contrary, the amplitude of inverted pendulum motion is low under large force in the y-axis direction. As the magnet distance changes, the torque direction of the magnetic particle changes in x-z plane, therefore the center of dx is going to change as the force changes.

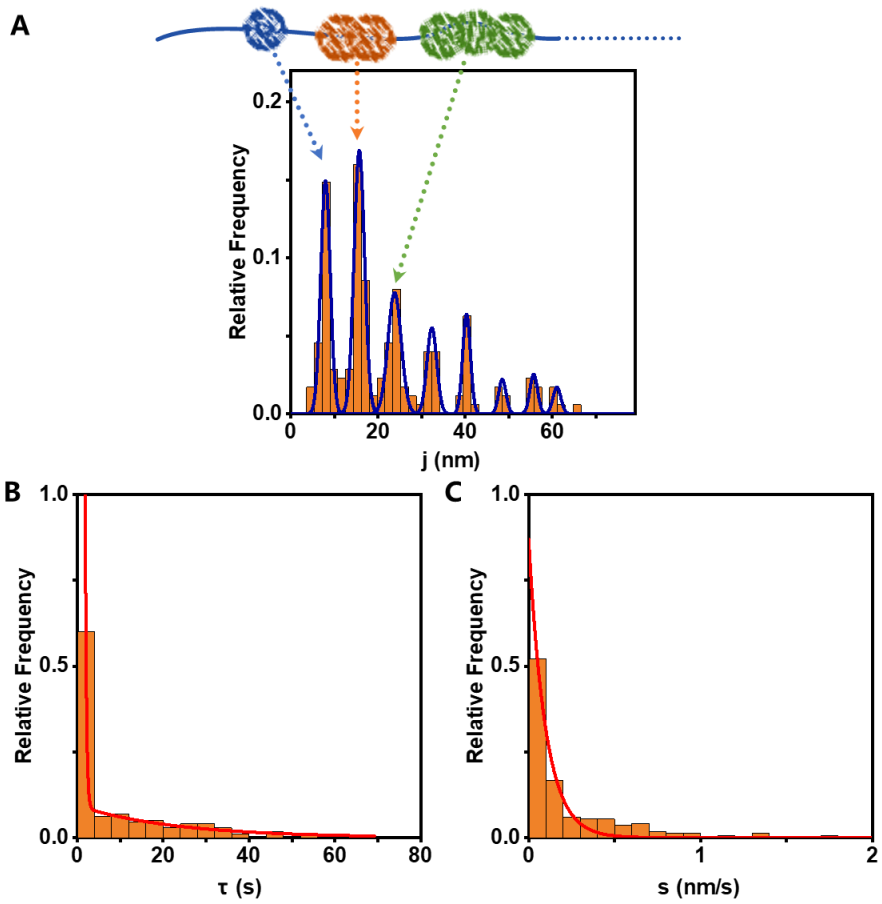

Figure S2. Statistical analysis of the unfolding parameters (R0-T3) of PNIPAM globule. The jump length j, waiting time τ, and expansive slope s were obtained from temperature-driven collapse at 42.5℃ and 3 pN pulling force (R0-T3). **(A)** Histograms of jump length j from 175 jump events. The blue lines show Gaussian fits. Under ~3 pN, the jump length of nucleus (the first peak position) is 8.0 ± 1.1 nm which is equivalent to 32 ± 4 monomers. The lengths of bigger collapsed structures are still multiple of the nucleus. The external force change (e.g., from 6 pN to 3 pN) doesn't affect the collapsed structure. The blue, orange and green blobs represent the beads containing one, two and three nuclei. (**B**) Histograms of unfolding waiting time τ of collapsed structures. The waiting time τ between successive unfolding steps is the lifetime of a bead and reflects the structure's kinetic stability. Our results show that τ follows a multiexponential distribution (at least two exponents), suggesting that the kinetics of bead unfolding involve multiple rate-limiting steps. The average waiting time was ~8.4 s, corresponding to an unfolding rate of ~0.12 s^{-1}. (**C**) Histograms of waiting-period-expansive slope s under 3 pN. The red line shows a single exponential fit. Because the slope s corresponds to a bead's expansion rate in the physical dimension during the globule-to-coil transition, it reflects the structural looseness.

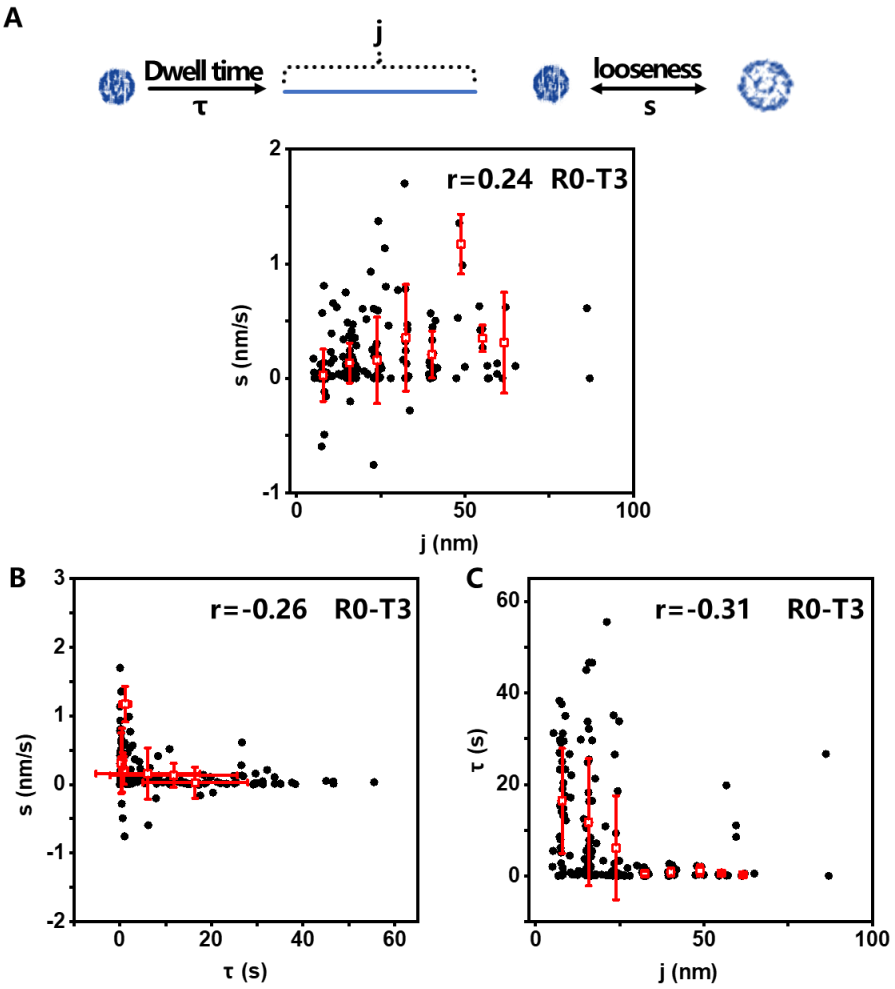

Figure S3. The correlation plots and Pearson's correlation coefficients r of (**A**) j-s, (**B**) τ-s, and (**C**) j-τ obtained from temperature-driven collapsed structures at 42.5℃ under 3 pN (R0-T3). Consistently, j, τ, s, and their correlation followed the same trend as that of R0-T6. For the individual wait-and-jump events, the jump length j is positively correlated with the expansion rate s (r = 0.24), indicating that collapsed structure with larger jump length j is relatively looser. This also proves that larger j values arise from unfolding of larger structures rather than simultaneous unfolding of the same structures. Consistently, the slope s is anticorrelated (r = -0.26) with the waiting time τ because looser beads (larger s) are expected to unfold faster (shorter τ). The jump length j is also anticorrelated with the waiting time τ (r = -0.31), which indicates that the smaller the collapsed structure is, the denser and more stable the structure is.

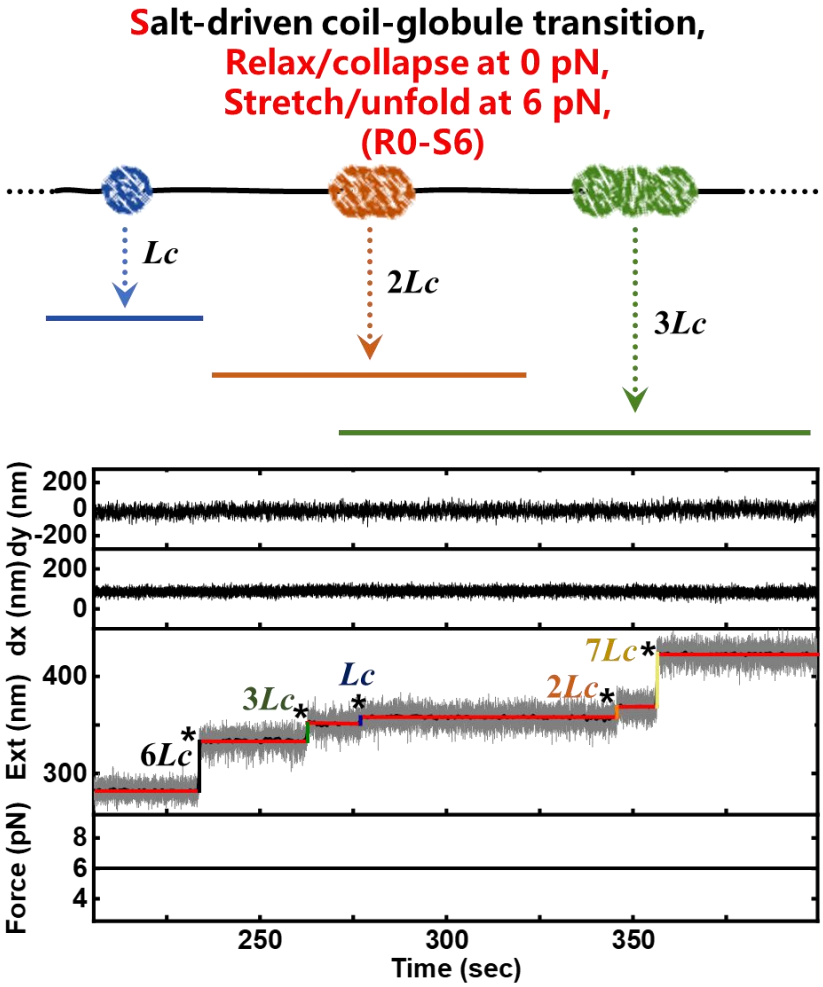

Figure S4. Typical real-time unfolding traces of salt-driven collapsed globule under constant force of 6 pN (R0-S6). The coil-globule transition is accomplished under high-salt condition without external force. Typical real-time traces obtained during the unfolding of a collapsed PNIPAM chain under a constant force of 6 pN (R0-S6). From the bottom to the top, the panels correspond to force-, extension-, dx- and dy- verse-time trajectories. Extension, dx and dy indicate z, x and y center positions of the tethered magnetic particle. Multiple steps of length jumps can be observed in the extension-time trace. The step sizes (*) show the unfolding of 5 structures in the collapsed globule including merged beads (2*Lc*, 3*Lc*, 6*Lc*, and 7*Lc*) and nucleus (*Lc*) under 6 pN constant force. It should be emphasized that it is normally difficult to unfold tandem repeat structures at the same time due to tiny local differences. The correlation between j and s also proves that larger j values arise from unfolding of larger structures rather than simultaneous unfolding of the same structures under constant force. And the center positions of dx and dy remain unchanged at constant force indicated the extension results from structures unfolding rather than interface interaction.

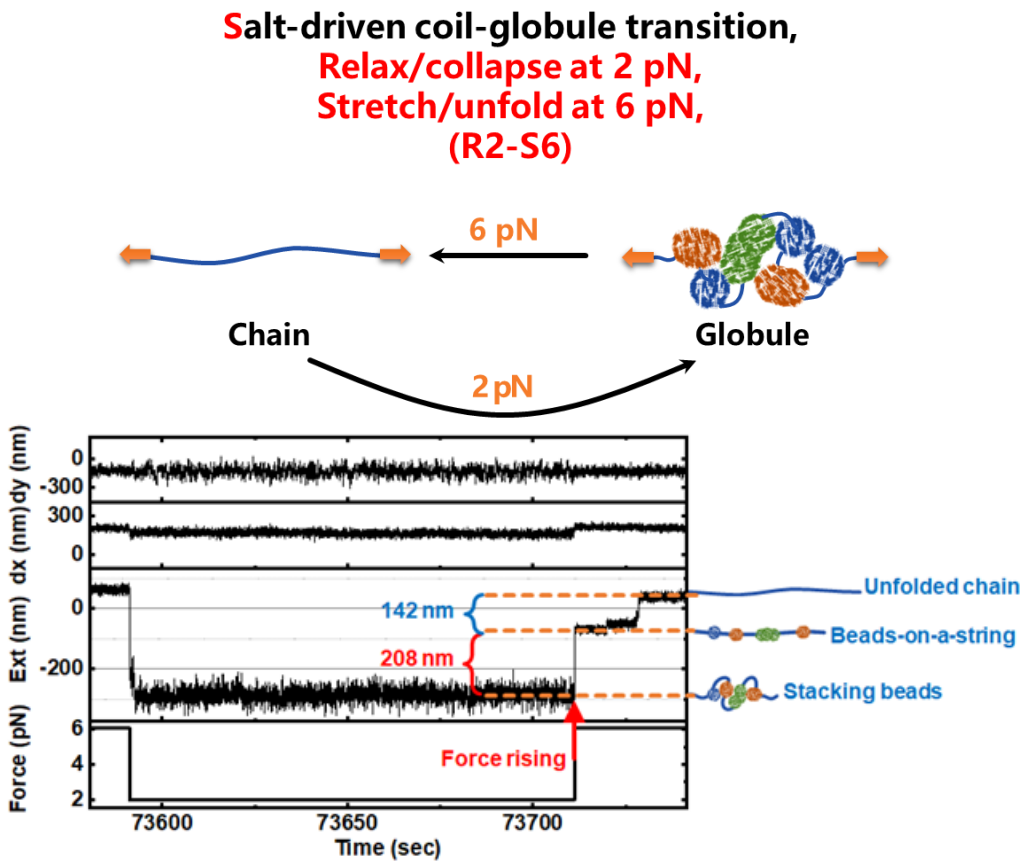

Figure S5. Typical real-time collapsing and unfolding traces of salt-driven collapsed polymer relaxed at 2 pN and then stretched at 6 pN (R2-S6). From the bottom to the top, the panels correspond to force-, extension-, dx- and dy- verse-time trajectories. Extension, dx and dy indicate z, x and y center positions of the tethered magnetic particle. The salt-driven coil-globule transition is accomplished at a constant force of 2 pN. During the unfolding of the globule under 6-pN external force sudden multi-step jumps appear. The unfolding curve of collapsed structure is also discontinuous and shows wait-and-jump steps. The magnetic particles can be seen as inverted pendulum in the magnetic. Under small pulling force (2 pN), the amplitude of inverted pendulum motion is high in the y-axis direction. On the contrary, the amplitude of inverted pendulum motion is low under large force (6 pN) in the y-axis direction. As the magnet distance (force) changes, the torque direction of the magnetic particle changes in x-z plane, therefore the center of dx is going to change as the force changes. Therefore, a deduction of length contribution from the magnetic particle rotation (~32 nm, see also Figure S10) from the first jump (208 nm, red arrow) produce the actual length increment of ~176 nm, which corresponds to the unraveling of a collapsed globule to the beads-on-a-string structure. While the subsequent step-wise unfolding at constant force (6 pN) produce a total length increment of 142 nm. The contribution of individual or merged nuclei to the whole structure of the globule is around 45%, which indicate that there exist free PNIPAM segments within the globule.

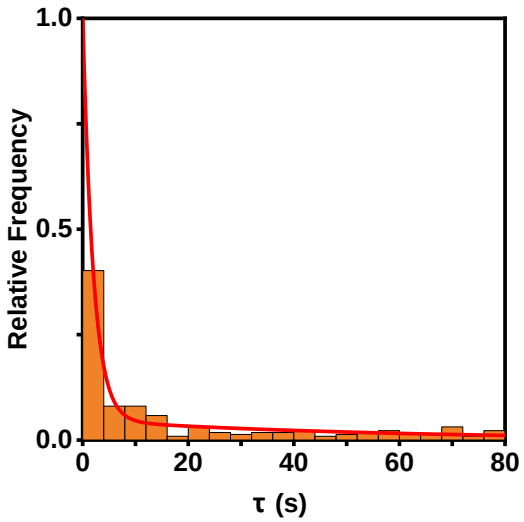

Figure S6. Histograms of unfolding waiting time τ of collapsed structures formed under 2 pN external force and stretched at 6 pN constant force (R2-S6). The prior waiting time τ is the duration of a globule and reflects the globule's kinetic stability; it follows a multiexponential distribution, with at least two exponents (red line, double exponential fit), suggesting that either the kinetics of globule unraveling involves a multiple rate-limiting step, or individual globules have different unraveling kinetics.

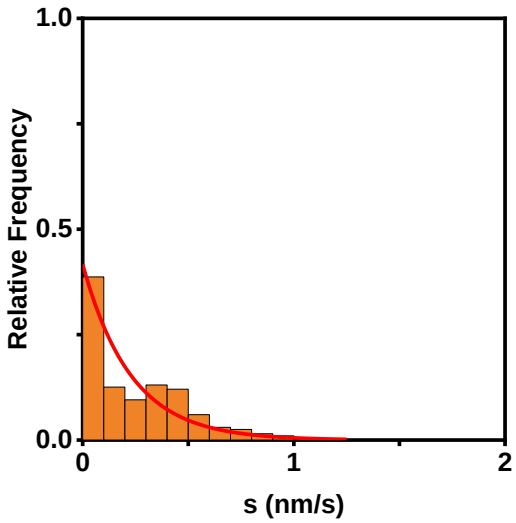

Figure S7. Histograms of waiting-period-expansive slopes of salt-driven collapsed structures formed at 2 pN and unfolded at 6 pN constant force (R2-S6). The expansive slope follows an exponential distribution (red line, single exponential fit).

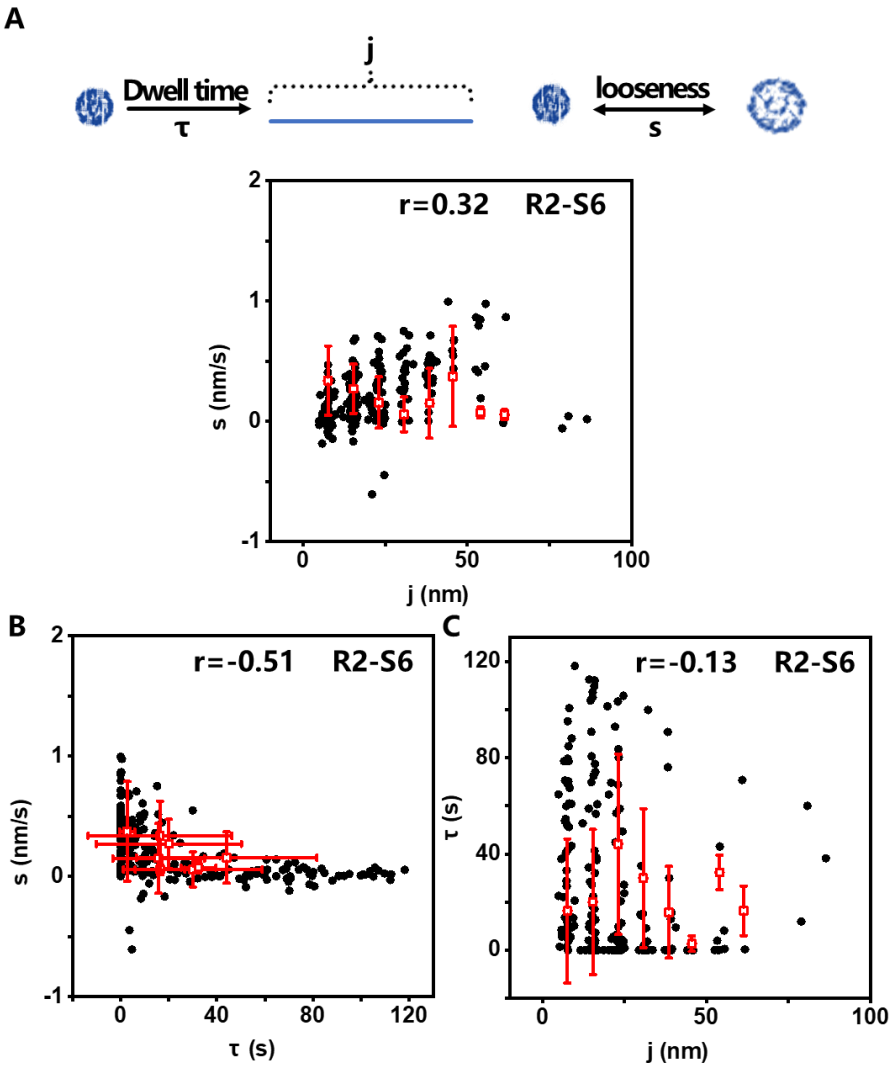

Figure S8. The correlation plots and Pearson's correlation coefficients r of (**A**) j-s, (**B**) τ-s and (**C**) j-τ from salt-driven collapsed polymer formed under a constant external force of 2 pN and unfolded at 6 pN constant force (R2-S6) in 0.3 M Na_2SO_4 buffer. Consistently, j, τ, s, and their correlation followed the same trend as that of R0-S6 (Figure S4). For the individual wait-and-jump events, the jump length j is positively correlated with the expansion rate s (r = 0.32), indicating that a structure with larger jump length j is looser. This also proves that larger j values arise from unfolding of larger structures rather than simultaneous unfolding of the same structures. Consistently, the slope s is anticorrelated (r = -0.51) with the waiting time τ because looser beads (larger s) are expected to unfold faster (shorter τ). The jump length j is also anticorrelated with the waiting time τ (r = -0.13), which indicates that the smaller the collapsed structure is, the denser and more stable the structure is.

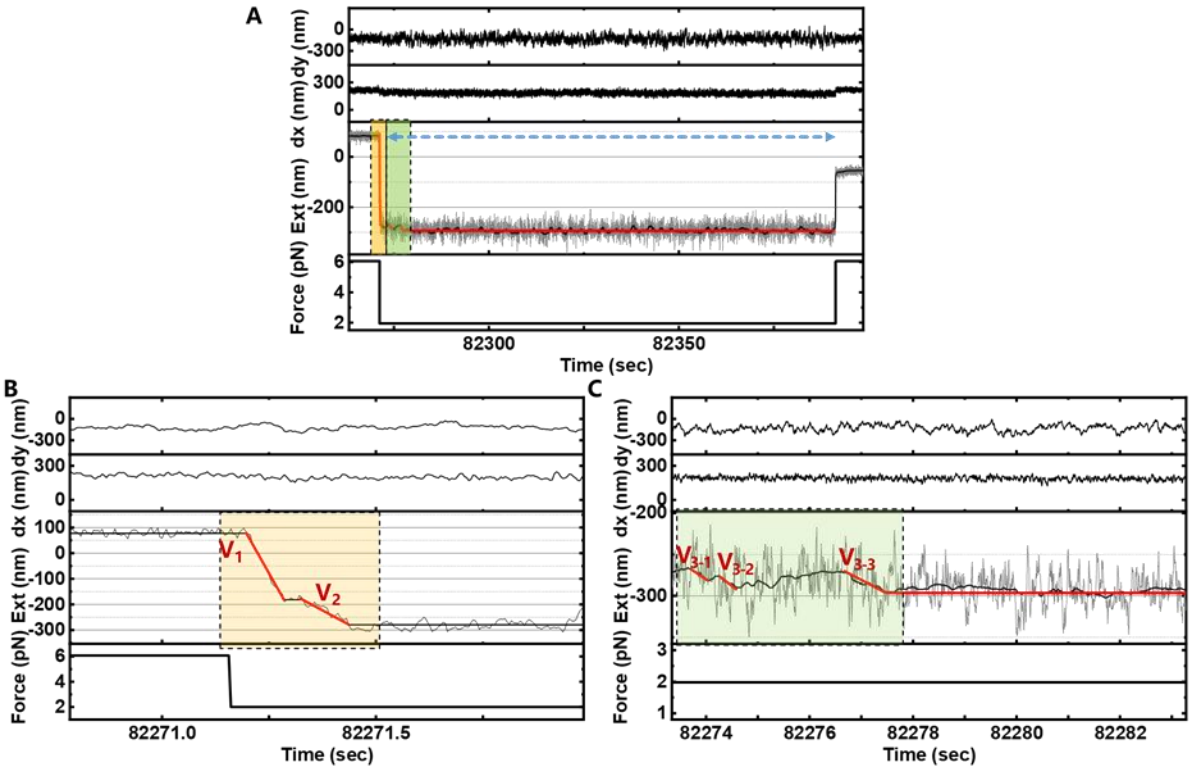

Figure S9. Monitoring the coil-globule transition process. Typical real-time traces obtained during the force stepping of 6 pN (unfolding) - 2 pN (collapsing) - 6 pN (unfolding) cycles in 0.3 M Na_2SO_4 (R2-S6). The individual PNIPAM chain was unraveled at 6 pN external force then the external force was switched to 2 pN for collapsing. From the bottom to the top, the panels correspond to force-, extension-, dx- and dy- verse-time trajectories. Extension, dx and dy indicate z, x and y center positions of the tethered magnetic particle. (**A**) A typical trajectory of a collapsing and unfolding process. (**B**) Enlarged view on the yellow areas in the (A). (**C**) Enlarged green areas in the (A). The coil-globule transition can cause the shortening of the apparent length of the polymer chain as indicated by the dashed blue line in Figure S9A. In addition, during the coil-globule transition, the collapsed curves of PNIPAM shows descending-and-wait steps as shown in yellow and green box (Figure S9B and Figure S9C).

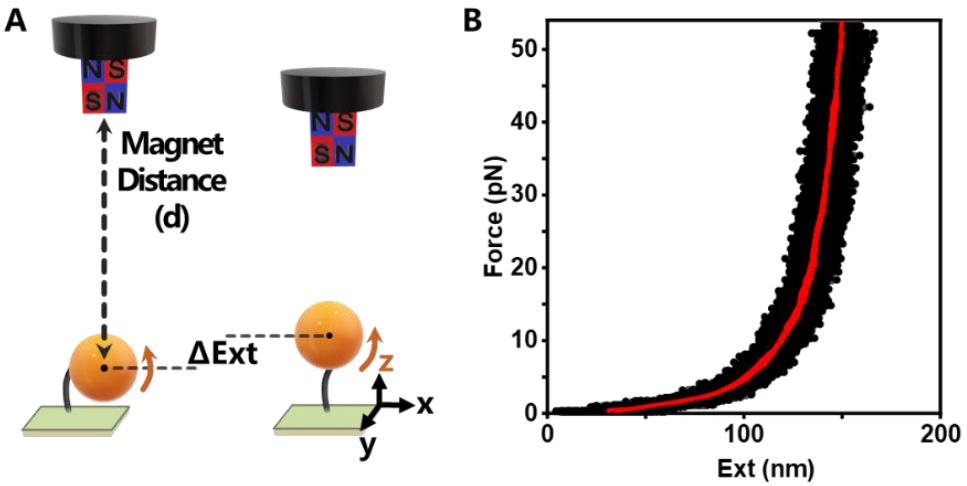

Figure S10. Calibration of the torque of the magnetic particle. (**A**) The schematic illustrations of the torque change of the magnetic particle with the change of magnet distance (external force). (**B**) The height correction curves of the magnetic particles' torsion. The red lines are the fitting of center position.

Section 2.2 AFM imaging of single-chain PNIPAM

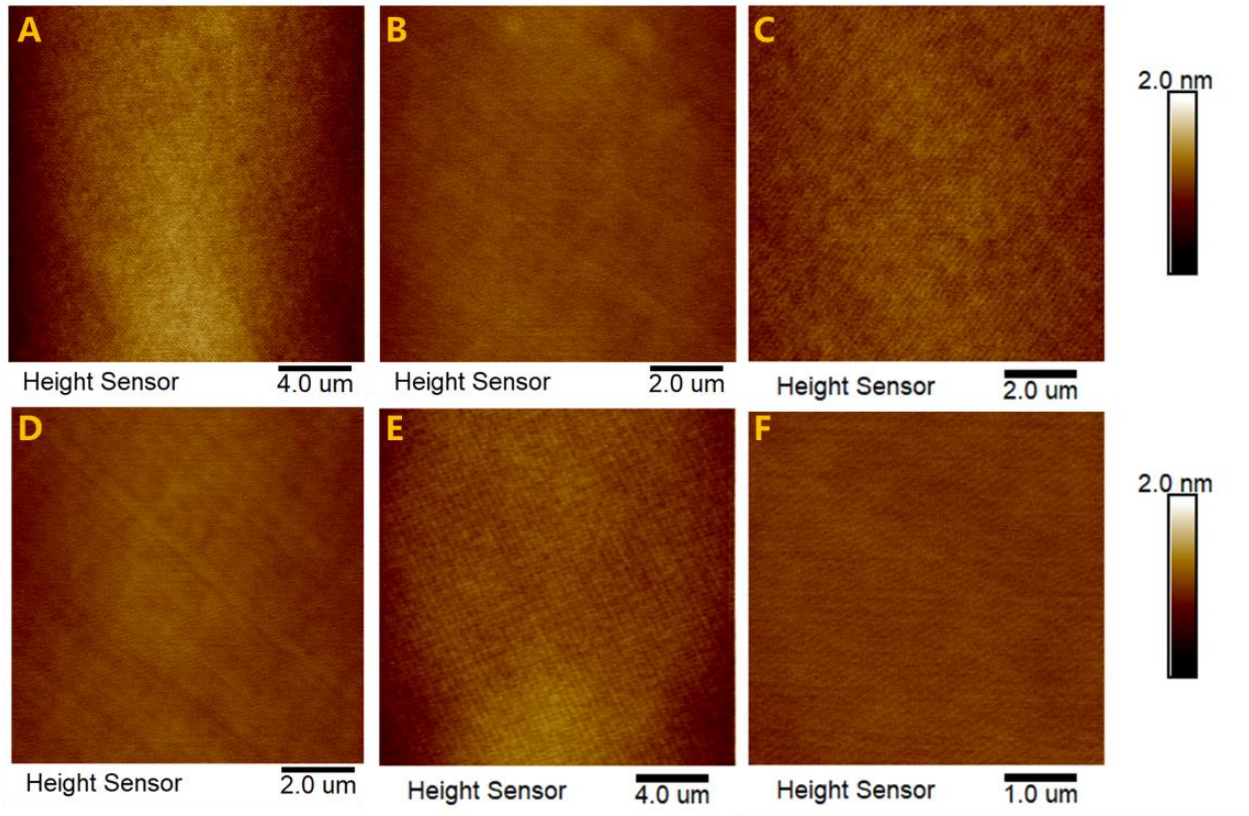

Figure S11. The AFM imaging of amino-group modified substrates. There is no visible aggregation in the amino-substrates.

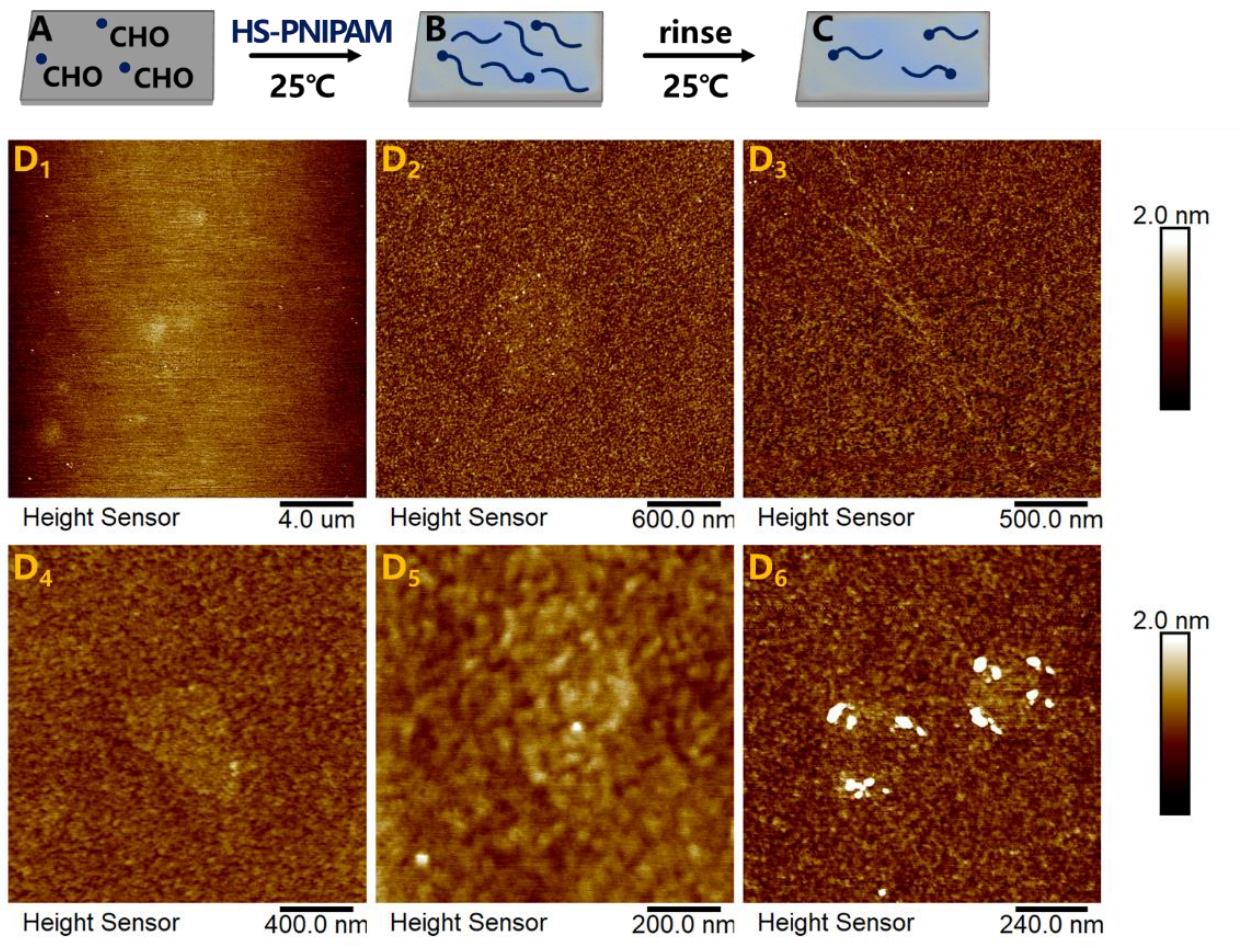

Figure S12. The air-phase AFM imaging of single-chain PNIPAM at room temperature. (**A-C**) Scheme of covalent immobilization of individual PNIPAM molecules on a solid substrate. The physisorbed PNIPAM was removed by vigorous rinsing with water. (**D_1-D_5**) The individual PNIPAM chains exhibit curl or extended coil conformations. (**D_6**) A partially collapsed PNIPAM chain due to dehydration or segment overlapping. It should be emphasized that water is a good solvent for PNIPAM at 25℃, and the low concentration (<10^{-8} g/mL) of PNIPAM can minimize intermolecular interactions and make the PNIPAM chain exist as isolated state at 25℃. As described in the literature, the higher capability of a flexible polymer to spread produces an extremely flat profile as shown in the Figure S12D_1-D_5. The individual polymers are mostly indistinguishable from the substrate due to a low height that is comparable to the substrate roughness and the finite dimensions of the tip. Occasionally, a couple of partially collapsed single-chains due to dehydration or overlapping can be detected, as shown in the Figure S12D_6.

Section 2.3 Synthesis and Characterization of PNIPAM

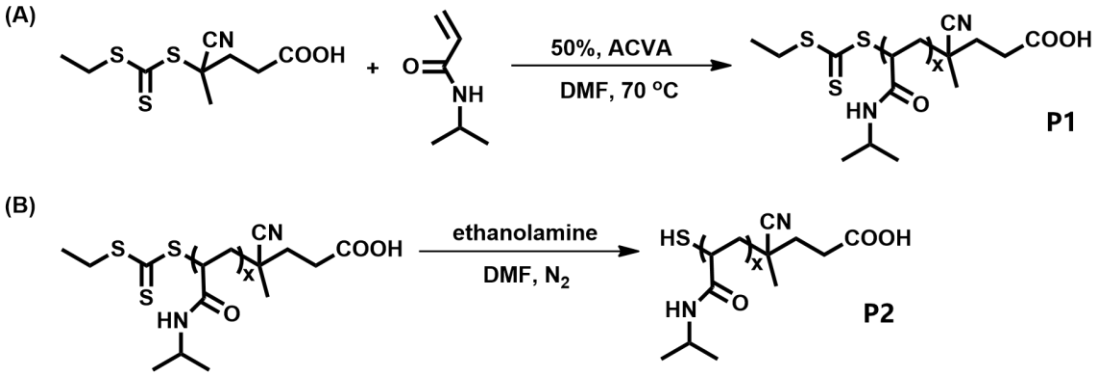

Figure S13. (**A**) Synthesis of PNIPAM homopolymer by RAFT polymerization and (**B**) aminolysis of PNIPAM homopolymer.

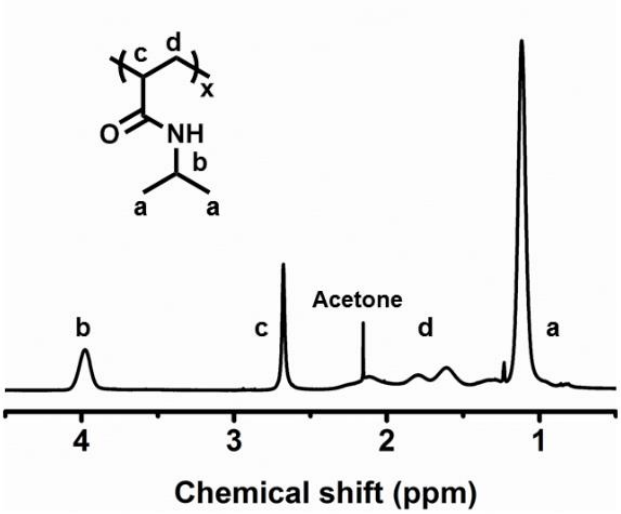

Figure S14. 400 MHz ^{1}H NMR spectrum of PNIPAM in $CDCl_3$. Characteristic ^{1}H NMR spectrum of PNIPAM: 4.1-3.9 ppm (s, -NCH-), 3.0-2.5 ppm (m, backbone -CH-), 2.0-1.3 ppm (m, backbone -CH_2-), 1.3-0.9 ppm (m, -CH_3).

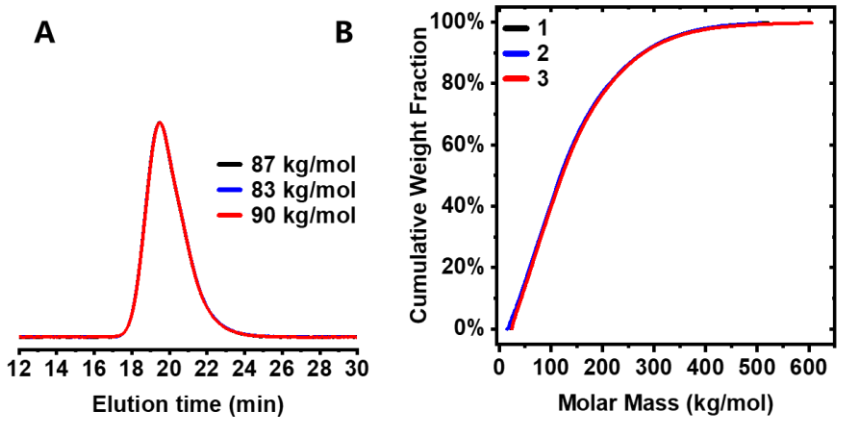

Figure S15. (**A**) GPC traces obtained from three independent measurements on the same batch of PNIPAM sample at a concentration of 2 mg/mL in DMF (LiBr). (**B**) The distribution of cumulative weight fraction of different molecular mass of PNIPAM.

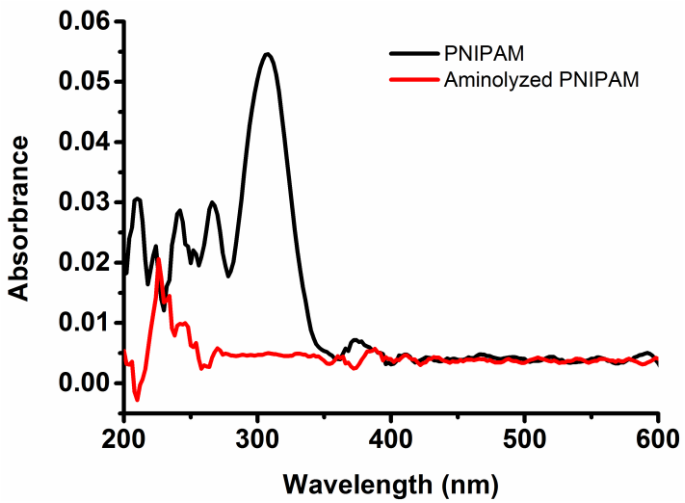

Figure S16. UV-vis spectra of PNIPAM (black trace) and aminolyzed PNIPAM (red trace) at a concentration of 3.0 mg/mL in DMF.

Section 2.4 The determination of LCST of PNIPAM

The transmittances of PNIPAM aqueous solutions at different temperatures were measured at 500 nm on UV-VIS spectrophotometer (UV-2450, SHIMADZU). The LCST was determined as a temperature exhibiting a 50% decrease in optical transmittance of the polymer solutions. The LCST of PNIPAM in pure PBS buffer and in the block buffer (PBS plus 1% tween-20) is the same, i.e., 30.5℃, which means the block buffer did not affect the LCST and coil-globule transition process of PNIPAM. While the LCST of PNIPAM in the purified water is 32.6℃. To make sure that the PNIPAM molecules immobilized on the solid substrate were completely collapsed into a globule structure, the temperature adopted during the magnetic tweezers experiments was kept at 42.5℃.

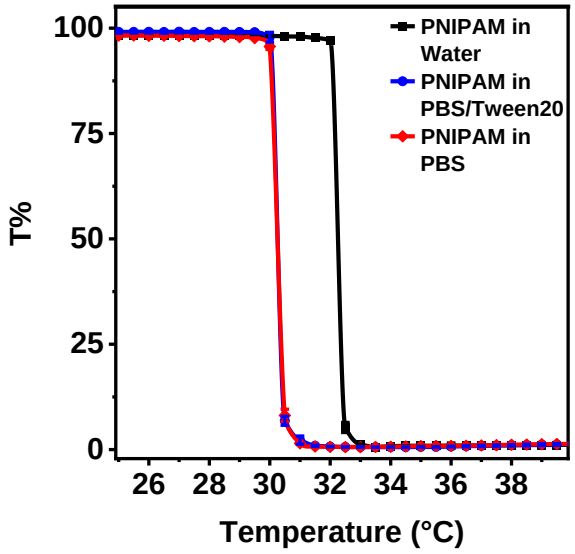

Figure S17. The transmittance of PNIPAM in water, PBS and PBS/1% tween-20 under different temperature.

Section 2.5 Single-molecule magnetic tweezers instrument and temperature-controller

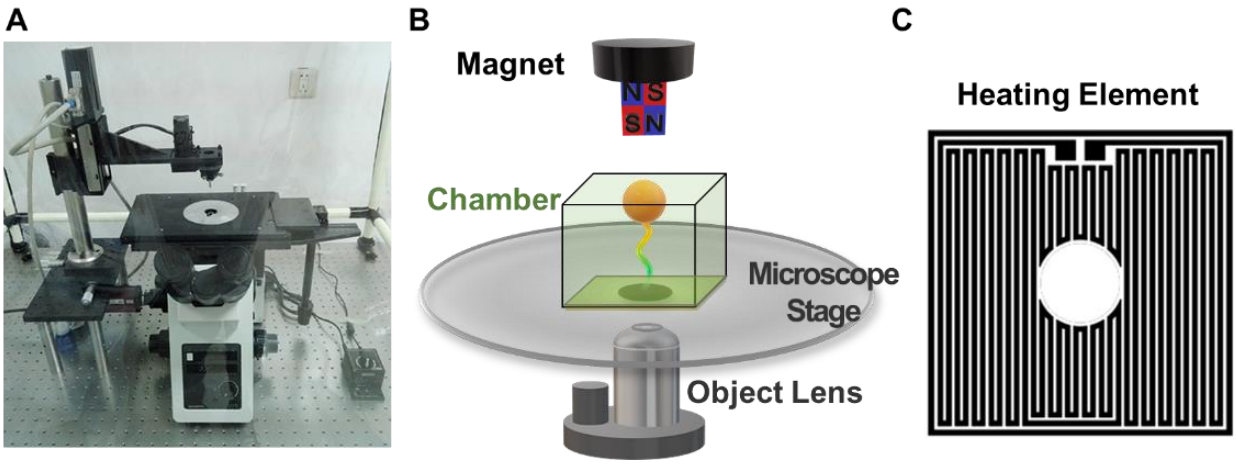

Figure S18. Instrument photo and diagram of magnetic tweezers. (**A**) The photo of Magnetic tweezers. (**B**) Schematic diagram of experimental operation area. (**C**) A homemade heating apparatus.

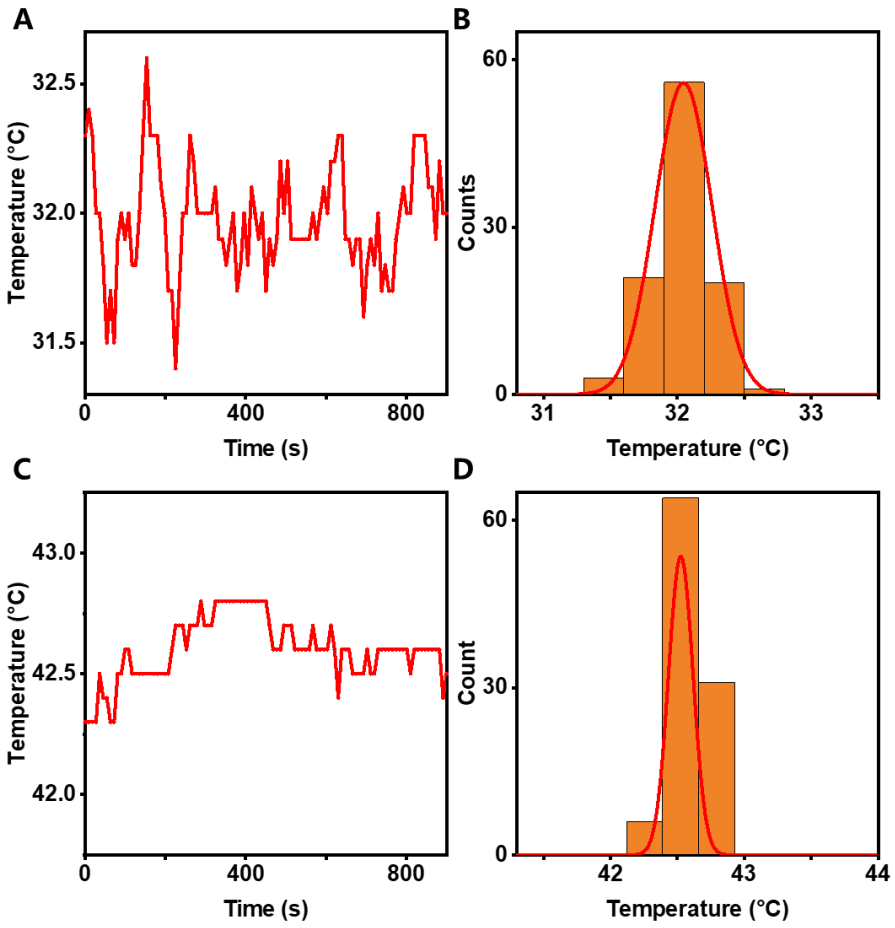

Figure S19. The measurement of temperature fluctuation for the home-made heating device. The target temperatures were set at 32 °C and 42.5 °C, respectively. The testing position is the experimental chamber. The testing environment and condition were the same as the MT experiment in this paper. The testing time of the two target temperatures was 900 seconds. **(A)** The real-time temperature during testing when target temperature was set at 32 °C. **(B)** Histograms of temperatures when target temperature was set at 32 °C. The red line shows Gaussian fits. The testing results are 32 ± 0.5℃. **(C)** The real-time temperature during testing when target temperature was set at 42.5 °C. **(D)** Histograms of temperatures when target temperatures was set at 42.5 °C. The red line shows Gaussian fits. The testing results are 42.5 ± 0.3℃. The testing results show the homemade heating device meet the requirement of magnetic tweezers based single molecule force spectroscopy.

Section 2.6 The criteria for multi-polymer tethering, surface detachment and single molecule stretching during magnetic tweezers experiment

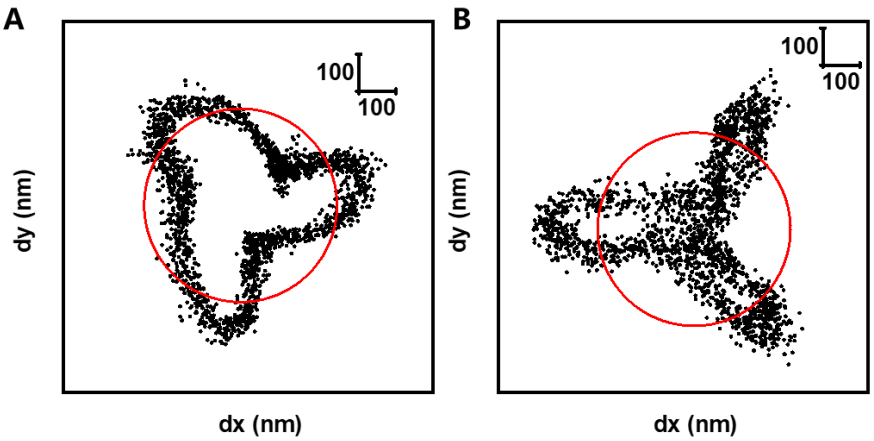

Figure S20. Examples of multi-polymer tethering. (**A, B**) Trajectory of x-y center position of multi-polymer tethered magnetic beads during magnets rotation before stretching. They show irregular movements. The red circle is manually added to the standard circle for reference. For the single-molecule tethered magnetic particles, the trajectory of the magnetic beads exhibited characteristic free rotation of a regular circle because of its uniform force in the x-y plane (Figure 1A, inset), whereas multiple-tethered particles show irregular movements.

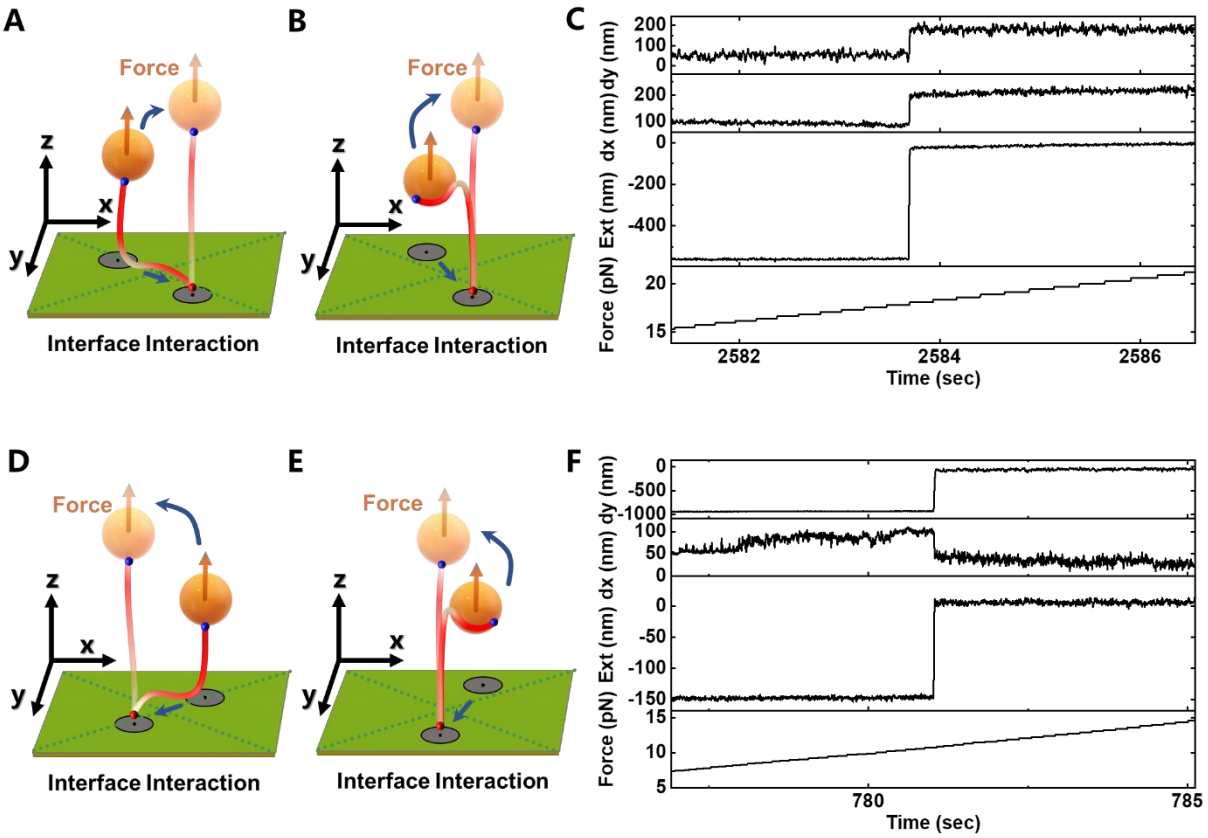

Figure S21. The criteria for the identification of polymer-substrate or polymer-magnetic bead interface interaction in the single-molecule magnetic tweezers experiments in water at 42.5 °C. Single PNIPAM chain was covalently tethered between the substrate and the magnetic particle as in the experiments. The gray circles on the substrates are the projection of the center position of the magnetic particle on the X-Y plane, and the center position of the gray circles is the coordinate values of the x and the y. (**A and D**) Scheme of different desorption directions from the substrate. (**B and E**) Scheme of different desorption directions from the magnetic particle. (**C and F**) The desorption traces for the case of (A, B) and (D, E), respectively. From the bottom to the top, the panels correspond to force-, extension-, dx- and dy- verse-time trajectories. Extension, dx and dy indicate z, x and y center positions of the tethered magnetic particle. The characteristic signal of interface interaction is the simultaneous change of three-dimensional coordinate. As the force exerted on the magnetic particle increases, the interfacial interaction on the molecular chains is desorbed, resulting in simultaneous changes in three-dimensional coordinates.

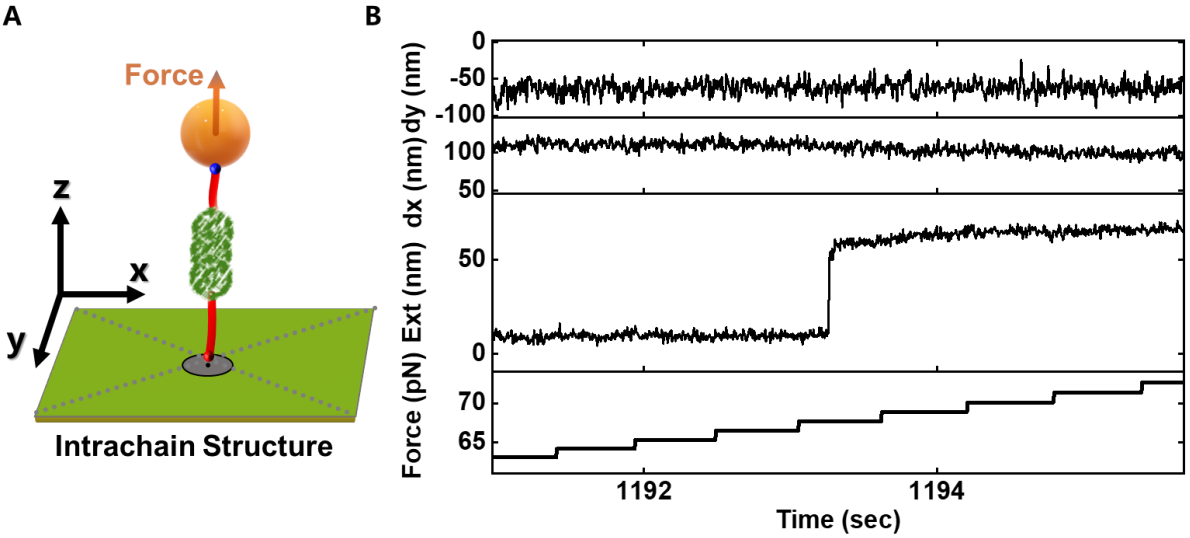

Figure S22. The stretching and unfolding of a free polymer with collapsed intrachain structure in water at 42.5 °C. Single PNIPAM chain was covalently tethered between the substrate and the magnetic particle as in the SMFS experiments. The gray circles on the substrates are the projection of the center position of the magnetic particle on the X-Y plane, and the center position of the gray circles is the coordinate values of the x and the y. **(A)** The schematic illustrations of the stretching. **(B)** The unfolding curves of collapsed polymer under pulling force. From the bottom to the top, the panels correspond to force-, extension-, dx- and dy- verse-time trajectories. Extension, dx and dy indicate z, x and y center positions of the tethered magnetic particle. The center positions of x-axis and the y-axis will keep constant, during the unfolding and sudden extension jump in z direction, which is different from the situation of surface detachment.

Table S1. The jump length and number of repeated units of temperature-driven collapsed PNIPAM structure measured at 42.5℃ under an external force of 3 pN (R0-T3). The jump length j is measured and analyzed statistically from extension-time curves of single molecule magnetic tweezers. The number of repeated units is determined according to the jump length. The smallest jump length is regarded as the size of nucleus. And the other bigger jump lengths were found to be comparable with the length of multiple nucleus (i.e., Expected number of repeated units).

Peak Number (R0-T3)	Jump length (nm)	Number of repeated units	Expected number of repeated units (multiple*nucleus)
1	8.0 ± 1.1	32 ± 4	32 (1*nucleus)
2	15.7 ± 1.2	62 ± 5	64 (2*nucleus)
3	23.8 ± 1.5	94 ± 6	96 (3*nucleus)
4	32.4 ± 1.1	129 ± 4	128 (4*nucleus)
5	40.3 ± 0.9	160 ± 4	160 (5*nucleus)
6	48.6 ± 0.4	193 ± 2	192 (6*nucleus)
7	55.8 ± 0.4	221 ± 2	224 (7*nucleus)
8	61.1 ± 0.4	242 ± 2	256 (8*nucleus)

Table S2. The jump length and number of repeated units of salt-driven (in 0.3 M Na_2SO_4) collapsed PNIPAM structure measured at room temperature relaxed at 0 pN and stretched at 6 pN constant force (R0-S6). The jump length j is measured and analysed statistically from extension-time curves of single molecule magnetic tweezers. The number of repeated units is determined according to the jump length. The smallest jump length is regarded as the size of nucleus. And the other bigger jump lengths were found to be comparable with the length of multiple nucleus (i.e., Expected number of repeated units).

Peak Number (R0-S6)	Jump length (nm)	Number of repeated units	Expected Number of repeated units (multiple*nucleus)
1	7.6 ± 1.2	30 ± 5	30 (1*nucleus)
2	14.5 ± 1.4	58 ± 6	60 (2*nucleus)
3	23.7 ± 1.0	94 ± 4	90 (3*nucleus)
4	30.7 ± 2.4	122 ± 10	120 (4*nucleus)
5	38.6 ± 1.1	153 ± 4	150 (5*nucleus)
6	46.9 ± 0.5	186 ± 2	180 (6*nucleus)
7	54.0 ± 0.5	214 ± 2	210 (7*nucleus)
8	62.9 ± 0.4	250 ± 2	240 (8*nucleus)

Table S3. The jump length and number of repeated units of salt-driven (in 0.3 M Na_2SO_4) collapsed PNIPAM structure measured at room temperature relaxed at 2 pN and stretched at 6 pN constant force (R2-S6). The jump length j is measured and analysed statistically from extension-time curves of single molecule magnetic tweezers. The number of repeated units is determined according to the jump length. The smallest jump length is regarded as the size of nucleus. And the other bigger jump lengths were found to be comparable with the length of multiple nucleus (i.e., Expected number of repeated units).

Peak Number (R2-S6)	Jump length (nm)	Number of repeated units	Expected Number of repeated units (multiple*nucleus)
1	7.8 ± 1.0	31 ± 4	31 (1*nucleus)
2	15.2 ± 1.0	60 ± 4	62 (2*nucleus)
3	23 ± 1.5	91 ± 6	93 (3*nucleus)
4	30.8 ± 1.0	122 ± 4	124 (4*nucleus)
5	38.7 ± 0.7	153 ± 3	155 (5*nucleus)
6	45.2 ± 0.4	179 ± 2	186 (6*nucleus)
7	53.9 ± 0.4	214 ± 2	217 (7*nucleus)
8	61.2 ± 0.4	242 ± 2	248 (8*nucleus)

References

(1) Shen, W.; Qiu, Q.; Wang, Y.; Miao, M.; Li, B.; Zhang, T.; Cao, A.; An, Z. Hydrazine as a nucleophile and antioxidant for fast aminolysis of raft polymers in air. *Macromol. Rapid Commun.* **2010**, *31*, 1444-1448, DOI: 10.1002/marc.201000154

(2) Skrabania, K.; Miasnikova, A.; Bivigou-Koumba, A. M.; Zehm, D.; Laschewsky, A. Examining the UV-vis absorption of RAFT chain transfer agents and their use for polymer analysis. *Polym. Chem.* **2011**, *2*, 2074-2083. DOI: 10.1039/C1PY00173F

(3) Liu, J.; Feng, W.; Zhang, W. A single-molecule study reveals novel rod-like structures formed by a thrombin aptamer repeat sequence. *Nanoscale* **2020**,*12*, 4159-4166, DOI: 10.1039/C9NR09054A

(4) Lee, M. S.; Kim, J. C.; Effects of surfactants on phase transition of poly(N-isopropylacrylamide) and poly(N-isopropylacrylamide-co dimethylaminoethylmethacrylate). *J. Dispers. Sci. Technol.* **2012**, *33*, 272-277, DOI: 10.1080/01932691.2011.561181

(5) Chen, H.; Fu, H.; Zhu, X.; Cong, P.; Nakamura, F.; Yan, J. Improved high-force magnetic tweezers for stretching and refolding of proteins and short DNA. *Biophys. J.* **2011**, *100*, 517-523. DOI: 10.1016/j.bpj.2010.12.3700

(6) Chen, H.; Yuan, G.; Winardhi, R. S.; Yao, M.; Popa, I.; Fernandez, J. M.; Yan, J. Dynamics of equilibrium folding and unfolding transitions of titin immunoglobulin domain under constant forces. *J. Am. Chem. Soc.* **2015**, *137*, 3540-3546, DOI: 10.1021/ja5119368

(7) You, H.; Wu, J.; Shao, F.; Yan, J. Stability and kinetics of C-MYC promoter G-quadruplexes studied by single-molecule manipulation. *J. Am. Chem. Soc.* **2015**, *137*, 2424-2427, DOI: 10.1021/ja511680u

(8) Liu, C.; Kubo, K.; Wang, E.; Han, K. S.; Yang, F.; Chen, G.; Escobedo, F. A.; Coates, G. W.; Chen, P. Single polymer growth dynamics. *Science* 2017, *358*, 352-355, DOI: 10.1126/science.aan6837

(9) Kolberg, A.; Wenzel, C.; Hackenstrass, K.; Schwarzl, R.; Ruttiger, C.; Hugel, T.; Gallei, M.; Netz, R. R.; Balzer, B. N. Opposing temperature dependence of the stretching response of single PEG and PNiPAM polymers. *J. Am. Chem. Soc.* **2019**, *141*, 11603-11613, DOI: 10.1021/jacs.9b04383

(10) Scotti, A.; Bochenek, S.; Brugnoni, M.; Fernandez-Rodriguez, M. A.; Schulte, M. F.; Houston, J. E.; Gelissen, A. P. H.; Potemkin, I. I.; Isa, L.; Richtering, W. Exploring the colloid-to-polymer transition for ultra-low crosslinked microgels from three to two dimensions. *Nat. Commun.* **2019**, *10*, 1418, DOI: 10.1038/s41467-019-09227-5